P H Y S I C A L R E V I E W L E T T E R S

Theory for Shock Dynamics in Particle-Laden Thin Films

Junjie Zhou,[1] B. Dupuy,[1] A. L. Bertozzi,[2] and A. E. Hosoi[1]

[1]*Department of Mechanical Engineering, Hatsopoulos Microfluids Laboratory, Massachusetts Institute of Technology,
77 Massachusetts Avenue, Cambridge, Massachusetts 02139, USA*
[2]*UCLA Mathematics Department, Box 951555, Los Angeles, California 90095-1555, USA*

We present a theory to explain the emergence of a particle-rich ridge observed experimentally in a thin film particle-laden flow on an incline. We derive a lubrication theory for this system which is qualitatively compared to preliminary experimental data. The ridge formation arises from the creation of two shocks due to the differential transport rates of fluid and particles. This parallels recent findings of double shocks in thermal-gravity-driven flow [A. L. Bertozzi *et al.*, Phys. Rev. Lett. **81**, 5169 (1998); J. Sur *et al.*, *ibid.* **90**, 126105 (2003); A. Münch, *ibid.* **91**, 016105 (2003)]. However, here the emergence of the shocks arises from a new mechanism involving the settling rates of the species.

Thin films have long been studied in a rich array of industrial, biological, and environmental contexts [1]. While extensive research has been conducted on clear fluids [2–6] and dry granular flows [7,8], far fewer studies have been dedicated to particle-laden fluid films. In applications such as debris flow [9,10], slurry transport, and mixing of pharmaceuticals, particles play a dominant role in the dynamics and cannot be neglected [11].

New and unexpected behavior is observed in these particulate systems owing to the introduction of a new time scale. In particle-laden, gravity-driven films [12], one time scale is associated with the viscous fingering that occurs at the contact line and a second is associated with particle settling. New and interesting phenomena arise when the two time scales are comparable, resulting in nonuniform particle distributions.

In clear fluid experiments involving flow on an inclined plane, the large scale dynamics is described by convective theory in which the first order terms in the equations of motion yield quantitative information about the speed and shape of the front. Recent results [13–15] show that temperature gradient driven flow balanced by gravity can be described by a scalar conservation law with a nonconvex flux. In the present study we find similar dynamics in particle-laden films. New phenomena are observed experimentally in the limit of high particle concentration and inclination angle, and this data is compared qualitatively to predictions arising from shock theory.

The experiment consists of an acrylic sheet with an adjustable inclination angle, β. A suspension of polydisperse glass beads (250–425 μm in diameter) flows from a reservoir (see Fig. 1). Profiles of the flowing layer at fixed y, as functions of x and time, are measured using a laser light sheet and a digital camera. Experiments were conducted using both wetting (Dow Corning 200, 1000 cSt fluid) and partially wetting (glycerol) fluids.

Three distinct regimes were observed experimentally (Fig. 2). At low inclination angles and concentrations,

sedimentation perpendicular to the plate occurs rapidly and particles are deposited in a uniform particulate front behind the advancing free surface. Clear fluid flows over the particulate matter and eventually fingers; the dynamics is precisely that observed in numerous clear fluid experiments (e.g., [2,16,17]). At high inclination angles and particle concentrations, the evolution deviates strikingly from the clear fluid case and a large particle-rich ridge appears at the advancing free surface front. The ridge observed in these dense suspensions may grow to several times the thickness of the trailing film. Between these two regimes, a well-mixed transition region appears, characterized by regular fingers containing particles. Intuitively we expect the large ridge to arise if the particle settling velocity along the plate exceeds that of the front.

To derive a model valid in the large-ridge region of parameter space, we consider the governing equations of motion for the mixture

$$\nabla \cdot \mathbf{\Pi} + \rho(\phi)\mathbf{g} = 0, \qquad \nabla \cdot \mathbf{j} = 0, \qquad (1)$$
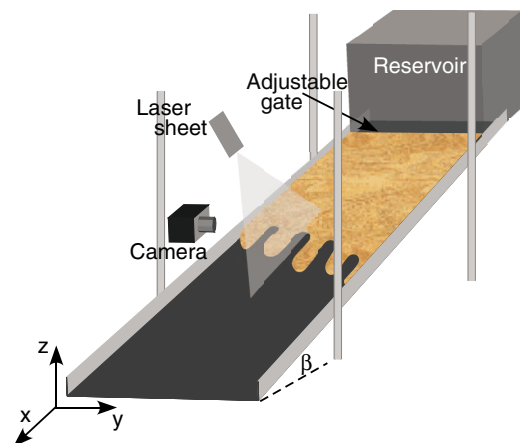

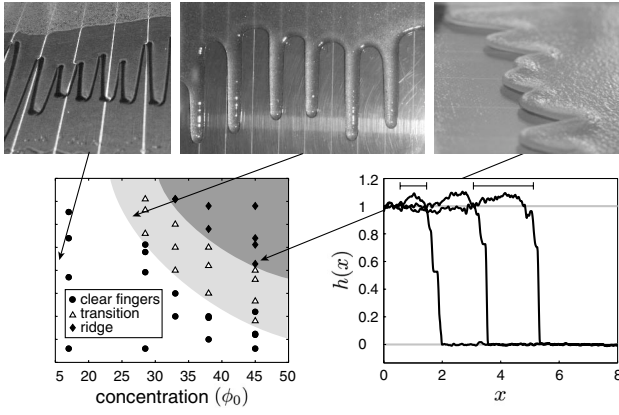FIG. 1 (color online).   Schematic of the experiment.

FIG. 2.   (Top) Photographs of typical fingering instabilities in each regime. (Bottom, left) Phase diagram for 250–425 μm beads in glycerol showing three regimes. (Bottom, right) Profiles of an advancing silicon oil front illustrating the widening ridge. Initial concentration $\phi_0 = 45\%$ and inclination angle $\beta = 42\,°$. Both axes are made dimensionless using H, the thickness of the film at the gate. Profiles are plotted every 30 sec.

where $\mathbf{j}$ is the volume averaged flux of the mixture, $\mathbf{g}$ is the acceleration of gravity, and $\mathbf{\Pi} = -p\mathbf{I} + \mu(\phi)(\nabla\mathbf{j} + (\nabla\mathbf{j})^T)$ is the stress tensor for the mixture. Here p is pressure, $\rho(\phi)$ and $\mu(\phi)$ are the effective density and viscosity, respectively, and $\mathbf{I}$ is the identity matrix. We consider low Reynolds number flows and neglect inertia of both the particulate and the fluid phase. The volume flux is related to the velocity by $\mathbf{j}_p = \phi\mathbf{v}_p$, $\mathbf{j}_f = (1 - \phi)\mathbf{v}_f$ and $\mathbf{j} = \mathbf{j}_p + \mathbf{j}_f$, where subscripts p and f refer to particle and fluid phase, respectively, and ϕ is the local particle concentration (by volume).

Particles move relative to the fluid phase via settling. This relative velocity is given by the Stokes settling velocity modified by two effects: (1) the presence of other particles in the dense suspension which hinders settling and (2) the no-slip boundary condition at the wall. To model the first, we adopt the Richardson-Zaki correction [18], valid for high concentrations, $\bar{f}(\phi) = (1 - \phi)^m$, where m is empirically determined to be ≈ 5.1. To capture the wall effect, we modify the Stokes settling velocity by a function that vanishes near the wall and approaches unity in the bulk flow [19]. Thus

$$\mathbf{v}_R = \frac{2}{9}\frac{(\rho_p - \rho_f)a^2}{\mu_f}\bar{f}(\phi)w(h)\mathbf{g}$$

where $\mathbf{v}_R$ denotes particle velocity relative to the fluid phase, a is a characteristic particle radius, μ_f is the viscosity of the fluid phase, ρ_f and ρ_p are the density of the fluid and particulate phase, respectively, and $w(h) \equiv \frac{Ah^2}{\sqrt{1 + (Ah^2)^2}}$. Here h is the local film thickness and A is a parameter that determines the sharpness of the transition from the no-slip wall to the bulk flow.

The effective mixture density $\rho(\phi) = \phi\rho_p + (1 - \phi)\rho_f$, and effective mixture viscosity [20]

$$\mu(\phi) = \mu_f(1 - \phi/\phi_{max})^{-2} \qquad (2)$$

are both functions of the local concentration. The viscosity diverges as the concentration approaches ϕ_{max} and the mixture becomes increasingly more solidlike.

At the substrate, we enforce a no-slip boundary condition. At the free surface, the normal stress balance is given by $\mathbf{n} \cdot \mathbf{\Pi} \cdot \mathbf{n} = \gamma\kappa$ and the tangential stress balance by $\mathbf{t} \cdot \mathbf{\Pi} \cdot \mathbf{n} = 0$ where $\mathbf{n}$ and $\mathbf{t}$ are, respectively, the unit outward normal and unit tangential vectors to the free surface, γ is the surface tension of the mixture (here assumed to be independent of particle concentration), and κ is the curvature of the free surface.

We begin by analyzing the 2D evolution of the film prior to the onset of fingering, neglecting variations in the y direction. Consider the following rescaling, motivated by the scaling adopted in gravity-driven clear fluid films [21]: $x = \tilde{x}L \equiv \tilde{x}(\ell^2 H/\sin\beta)^{1/3}$, $z = H\tilde{z}$, $p = P\tilde{p} \equiv \frac{\mu_f LU}{H^2}\tilde{p}$, $t = \tilde{t}T \equiv (3\mu_f/\gamma)(\ell^2 L/H^2\sin\beta)\tilde{t}$, and $(j^x, j^z) = U(\tilde{j}^x, \epsilon\tilde{j}^z)$. Here $\ell = \sqrt{\gamma/\rho_f g}$ is the capillary length, H is the thickness of the film far behind the moving front, dimensionless quantities are denoted by a tilde, and a characteristic velocity is defined as $U = L/T$. Equations (1) are rescaled using the above relations and we retain only the lowest order terms in $\epsilon \equiv H/L = (3Ca)^{1/3}$ where $Ca = \mu_f U/\gamma$ is the capillary number. If $\epsilon Pe \ll 1$, where $Pe = UH/D$ is the Peclet number and D is the diffusion coefficient for the particulate phase, particles diffuse rapidly across the depth of the film creating a uniform distribution in z; hence ϕ may be approximated as $\phi(x, t)$ [22]. Following a standard long wavelength approach for thin films (e.g., [4]), we solve for the velocities and pressures and depth average the equations bearing in mind that there are two mass conservation conditions, one for the mixture and one for the particles. Dropping the tildes, this yields two coupled equations for the evolution of ϕ and h:

$$\frac{\partial(\rho(\phi)h)}{\partial t} + \left\{\frac{\rho(\phi)}{\mu(\phi)}h^3 h_{xxx} - D(\beta)\left[\frac{\rho(\phi)}{\mu(\phi)}h^3(\rho(\phi)h)_x\right.\right.$$
$$\left.\left. - \frac{5}{8}\frac{\rho(\phi)}{\mu(\phi)}h^4(\rho(\phi))_x\right] + \frac{\rho(\phi)^2}{\mu(\phi)}h^3\right\}_x = 0 \quad (3)$$

$$\frac{\partial(\phi h)}{\partial t} + \left\{\frac{\phi}{\mu(\phi)}h^3 h_{xxx}\right.$$
$$- D(\beta)\left[\frac{\phi}{\mu(\phi)}h^3(\rho(\phi)h)_x - \frac{5}{8}\frac{\phi}{\mu(\phi)}h^4(\rho(\phi))_x\right]$$
$$\left. + \frac{\phi\rho(\phi)}{\mu(\phi)}h^3 + \frac{2}{3}V_s\phi h f(\phi)w(h)\right\}_x = 0 \qquad (4)$$

where $V_s \equiv \frac{\rho_p - \rho_f}{\rho_f}\frac{a^2}{H^2}$, $D(\beta) \equiv (3Ca)^{1/3}\cot(\beta)$, subscripts

denote partial derivatives, and we have absorbed the extra factor of $(1 - \phi)$ into f by defining $f(\phi) \equiv (1 - \phi)\bar{f}(\phi)$.

To determine macroscopic properties of the flow, it is instructive to investigate the underlying convective dynamics, described by the system of two conservation laws:

$$\frac{\partial(\rho(\phi)h)}{\partial t} + \left\{\frac{\rho(\phi)^2}{\mu(\phi)}h^3\right\}_x = 0 \qquad (5)$$

$$\frac{\partial(\phi h)}{\partial t} + \left\{\frac{\phi\rho(\phi)}{\mu(\phi)}h^3 + \frac{2}{3}V_s\phi h f(\phi)w(h)\right\}_x = 0. \qquad (6)$$

Consider as an initial condition a jump in the height from 1 to the precursor thickness b, and a constant concentration of ϕ_0. That is, at time zero, $h = 1$ for $x \leq 0$, $h = b$ for $x > 0$, and $\phi(x) = \phi_0$. The above system has the form of a 2×2 system of scalar conservation laws

$$\frac{\partial u}{\partial t} + [F(u, v)]_x = 0, \qquad \frac{\partial v}{\partial t} + [G(u, v)]_x = 0, \qquad (7)$$

where $u = \rho h$ and $v = \phi h$. The initial condition gives us a Riemann problem, i.e., both of the system variables u and v have a jump at the origin at time zero. Classical solutions of this problem, when they exist, are well-known in the theory of shock waves [23]. An intermediate state (u_i, v_i) emerges separating the left state $(u_l, v_l) = (\rho_f\rho(\phi_0), \phi_0)$, from the right state $(u_r, v_r) = (\rho_f\rho(\phi_0)b, \phi_0 b)$. The values u_i and v_i determine the density of particles, ϕ_i, and the fluid thickness, h_i, in the ridge (see Fig. 4, left).

A general 2×2 system of conservation laws (7) is hyperbolic if the Jacobian matrix

$$J(u, v) = \begin{pmatrix} F_u & F_v \\ G_u & G_v \end{pmatrix}$$

has two real distinct eigenvalues $\lambda_1(u, v)$ and $\lambda_2(u, v)$, with eigenvectors r_1, r_2. The problem is called genuinely nonlinear if $r_i \cdot \nabla\lambda_i \neq 0$, where the gradient is with respect to the variables u and v. For a large range of relevant physical parameters in (5) and (6), both conditions are satisfied provided we include the wall function $w(h)$. Setting $w(h) = 1$ results in a change in hyperbolicity of (5) and (6) at small h.

Under the assumptions of hyperbolicity and genuine nonlinearity, there is a methodology for determining the intermediate values u_i and v_i in terms of the left and right states. Thus, for a fixed concentration in the reservoir and upstream film thickness, given the particle concentration and thickness of the precursor film, we can find the height, concentration and propagation speed of the ridge. A one parameter family of shock solutions, connecting (u_i, v_i) to (u_l, v_l) or (u_r, v_r) can be determined by recognizing that the weak form of (7) yields two Rankine-Hugoniot conditions for the shock speed both of which have to be satisfied. For the 1-shock, connecting (u_l, v_l) to (u_i, v_i), we have

$$s_1 = \frac{F(u_i, v_i) - F(u_l, v_l)}{u_i - u_l} = \frac{G(u_i, v_i) - G(u_l, v_l)}{v_i - v_l} \qquad (8)$$

which gives two equations in three unknowns. Analogous formulas hold for the 2-shock connecting (u_i, v_i) to (u_r, v_r). This gives a total of four equations and four unknowns, namely s_1, s_2, u_i, and v_i. Generically there will be a locally unique solution, however these equations are also accompanied by entropy conditions which restrict whether a 1-shock or 2-shock is an admissible connection. In the case of the 1-shock, the entropy condition is $\lambda_{1l} < s_1 < \lambda_{1i}$ and $\lambda_{2l}, \lambda_{2i} > s_1$. For the 2-shock we require $\lambda_{2l} < s_2 < \lambda_{2i}$ and $\lambda_{1l}, \lambda_{1i} < s_2$ (see [23] for details). In the results presented here, the entropy condition is satisfied for both the 1- and 2-shocks and the shock connection problem can be solved numerically, providing an implicit formula for determining the intermediate state (u_i, v_i) that emerges from the Riemann initial data.

Numerical simulations show that the reduced model (5) and (6), captures the large scale dynamics of the full equations, (3) and (4), including the shock speeds s_1 and s_2 and ridge height h_i and ridge particle concentration ϕ_i.
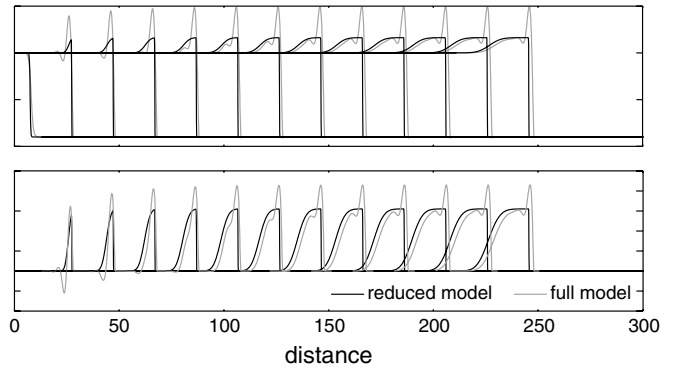
FIG. 3. Full and reduced model numerical profiles for $\phi_0 = 30\%$. (Top) Comparison of height profiles of the full system (3) and (4) with the reduced system (5) and (6). (Bottom) Concentration profiles for the full system (3) and (4) and the reduced system (5) and (6). Profiles are plotted at 40 sec intervals. The large spike at the leading edge of the full system corresponds to a capillary ridge due to surface tension.
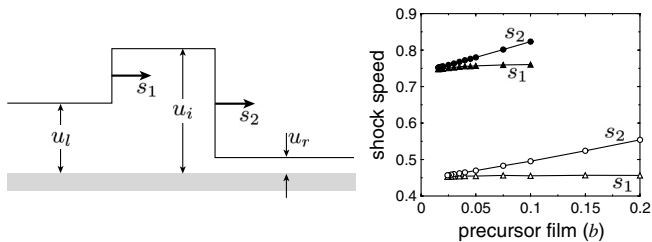

FIG. 4. (Left) Schematic diagram of the connection problem. (Right) Shock speeds calculated via the connection problem as a function of precursor thickness for $\phi_0 = 15\%$ (filled symbols) and $\phi_0 = 30\%$ (open symbols).

TABLE I. Comparison of shock speeds and intermediate states in model simulations and shock theory. Data shown for $\phi_0 = 0.30$, $b = 0.1$. Quantitative experimental data is not presented here owing to the sensitive dependence on precursor film as discussed in the text.

	Full Model	Reduced Model	Shock Theory
h_i	1.15	1.162	1.1619
ϕ_i	0.359	0.362	0.3620
s_1	0.435	0.434	0.4556
s_2	0.498	0.493	0.4956

The numerical methods used are an explicit upwind for (5) and (6) and backward Euler with spatial centered differences for (3) and (4). Figure 3 shows a sample calculation with parameters $m = 5$, $\phi_{\max} = 0.67$, $\phi_0 = 0.3$, $b = 0.1$, $\beta = 90°$, and $A = 0.5$. The large spike at the leading edge of the full system solution corresponds to the capillary ridge due to surface tension, which is neglected in the reduced system. In both solutions, an intermediate state appears connecting the left and right states via shocks. The trailing shock in Fig. 3 is smeared out due to numerical diffusion. Note that while the capillary ridge of the full system propagates with a fixed width, the particle-rich region between the two shocks continues to broaden as seen in the experiment. The full lubrication theory, reduced model and shock connection problem all consistently predict the formation of a large particle-rich ridge at high inclination angles and high concentrations. The numerically observed values in the full and reduced model are compared with the results from the connection problem in Table I. All three models display a sensitive dependence on the precursor thickness making quantitative comparison with experimental data challenging.

This sensitivity is illustrated in the shock speeds shown in Fig. 4, right, in which s_1 and s_2 are shown to converge as b decreases. We also observe h_i to increase as b decreases. This presents a marked contrast to the clear fluid case in which the front speed does not depend in a singular way on the precursor thickness. Moreover, the logarithmic dependence of the capillary ridge on b for the clear fluid problem may be complicated by the sensitivity of the underlying particle transport problem to the precursor thickness. The strong influence of the precursor on the basic flow structure (without surface tension effects) underscores the need for more detailed experimental measurements. Specifically, quantitative comparison between theory and experiment requires precise measurements of the precursor thickness and shock separation over time.

Shock theory for *systems* of conservation laws is well-known in gas dynamics but has never before been applied to the physics of contact lines. This new theory suggests many avenues for further study including the dependence of the dynamics on contact line physics, and the extension of the theory to the transverse direction to address the development of fingers, which appear to be somewhat suppressed in the experiment by the formation of the particle-rich ridge.

[1] T. G. Myers, SIAM Rev. **40**, 441 (1998).
[2] H. E. Huppert, Nature (London) **300**, 427 (1982).
[3] S. M. Troian, E. Herbolzheimer, S. A. Safran, and J. F. Joanny, Europhys. Lett. **10**, 25 (1989).
[4] A. Oron, S. H. Davis, and S. G. Bankoff, Rev. Mod. Phys. **69**, 931 (1997).
[5] Y. Ye and H.-C. Chang, Phys. Fluids **11**, 2494 (1999).
[6] L. Kondic and J. Diez, Phys. Fluids **13**, 3168 (2001).
[7] O. Pouliquen, J. Delour, and S. B. Savage, Nature (London) **386**, 816 (1997).
[8] S. B. Savage and K. Hutter, J. Fluid Mech. **199**, 177 (1989).
[9] J. E. Simpson, *Gravity Currents in the Environment and the Laboratory* (Cambridge University Press, Cambridge, England, 1997), 2nd ed.
[10] R. M. Iverson, Rev. Geophys. **35**, 245 (1997).
[11] R. H. Davis and A. Acrivos, Annu. Rev. Fluid Mech. **17**, 91 (1985).
[12] L. Xianfan and C. Pozrikidis, Philos. Trans. R. Soc. London A **361**, 847 (2003).
[13] A. L. Bertozzi, A. Münch, X. Fanton, and A. M. Cazabat, Phys. Rev. Lett. **81**, 5169 (1998).
[14] J. Sur, A. L. Bertozzi, and R. P. Behringer, Phys. Rev. Lett. **90**, 126105 (2003).
[15] A. Münch, Phys. Rev. Lett. **91**, 016105 (2003).
[16] M. F. G. Johnson, R. A. Schluter, M. J. Miksis, and S. G. Bankoff, J. Fluid Mech. **394**, 339 (1999).
[17] J. M. Jerrett and J. R. de Bruyn, Phys. Fluids A **4**, 234 (1992).
[18] J. F. Richardson and W. N. Zaki, Trans. Inst. Chem. Eng. **32**, 35 (1954).
[19] For a single particle settling near a vertical wall, the settling speed correction can be calculated analytically via the method of images [see, e.g., J. Happel and H. Brenner. *Low Reynolds Number Hydrodynamics* (Prentice-Hall Inc., Englewood Cliffs, NJ, 1965)].
[20] J. F. Brady, J. Chem. Phys. **99**, 567 (1993).
[21] A. L. Bertozzi and M. P. Brenner, Phys. Fluids **9**, 530 (1997).
[22] This assumption is violated in the clear finger regime in which the concentration approaches $\phi_{\max}$ at $z = 0$ and 0 at $z = h$. However, we restrict our analysis to the high angle, high concentration regime where the $\phi = \phi(x, t)$ assumption is valid.
[23] P. D. Lax, *Hyperbolic Systems of Conservation Laws and Mathematical Theory of Shock Waves*, CBMS-NSF Regional Conference Series in Applied Mathematics Vol. 11 (SIAM, Philadelphia, 1973).